

## First-principles study of intersite magnetic couplings in $\text{NdFe}_{12}$ and $\text{NdFe}_{12}\text{X}$ ( $\text{X} = \text{B}, \text{C}, \text{N}, \text{O}, \text{F}$ )

Taro Fukazawa,<sup>1,2, a)</sup> Hisazumi Akai,<sup>3,2</sup> Yosuke Harashima,<sup>1,2</sup> and Takashi Miyake<sup>1,2</sup>

<sup>1)</sup>*CD-FMat, National Institute of Advanced Industrial Science and Technology, Tsukuba, Ibaraki 305-8568, Japan*

<sup>2)</sup>*ESICMM, National Institute for Materials Science, Tsukuba, Ibaraki 305-0047, Japan*

<sup>3)</sup>*The Institute for Solid State Physics, The University of Tokyo, 5-1-5 Kashiwanoha, Chiba, Japan*

(Dated: 10 March 2022)

We present a first-principles investigation of  $\text{NdFe}_{12}$  and  $\text{NdFe}_{12}\text{X}$  ( $\text{X} = \text{B}, \text{C}, \text{N}, \text{O}, \text{F}$ ) crystals with the  $\text{ThMn}_{12}$  structure. Intersite magnetic couplings in these compounds, so-called exchange couplings, are estimated by Liechtenstein's method. It is found that the Nd-Fe couplings are sensitive to the interstitial dopant X, with the Nd-Fe(8j) coupling in particular reduced significantly for  $\text{X} = \text{N}$ . This suggests that the magnetocrystalline anisotropy decays quickly with rising temperature in the  $\text{X} = \text{N}$  system although nitrogenation has advantages over the other dopants in terms of enhancing low-temperature magnetic properties. The Curie temperature is also calculated from the magnetic couplings by using the mean field approximation. Introduction of X enhances the Curie temperature, with both structural changes and chemical effects found to play important roles in this enhancement.

PACS numbers: 75.50.Ww, 75.50.Bb, 71.20.Be, 71.20.Eh, 71.15.Mb

Keywords: Hard magnet, Permanent magnet, First-principles calculation,  $\text{NdFe}_{12}\text{N}$ ,  $\text{ThMn}_{12}$ -type structure

---

<sup>a)</sup>E-mail: taro.fukazawa@aist.go.jp

## I. INTRODUCTION

The magnetic compound  $\text{NdFe}_{12}\text{N}$ , which has the  $\text{ThMn}_{12}$  tetragonal structure, has attracted much attention since Hirayama et al.<sup>1,2</sup> successfully synthesized the compound—motivated by the results of a first-principles calculation<sup>3</sup>—and found that it has higher spontaneous saturation magnetization and anisotropy field than  $\text{Nd}_2\text{Fe}_{14}\text{B}$ .  $\text{NdFe}_{12}$  was first synthesized on a substrate, and then nitrogen was introduced. The nitrogenation greatly enhanced the magnetization and anisotropy field<sup>1</sup>; nitrogenation is known to have this effect in other similar magnetic compounds also. Although it has not been reported in the case of  $\text{NdFe}_{12}$ , typical elements can also enhance the Curie temperature of rare-earth magnets. For example, simultaneous enhancement of saturation magnetization and the Curie temperature has been experimentally observed in  $\text{R}_2\text{Fe}_{17}\text{C}_x$  (Ref. 4 and 5),  $\text{R}_2\text{Fe}_{17}\text{N}_x$  (Ref. 5), and  $\text{RTiFe}_{11}\text{N}_x$  (Ref. 6 and 7), where R denotes a series of rare-earth elements.

The advantages of typical elements in magnets have also been studied theoretically. Kanamori<sup>8,9</sup> discussed mixing of the  $d$ -states of transition metal sites with the states of neighboring atoms in compounds, and he suggested that the strong ferromagnetism in  $\text{Nd}_2\text{Fe}_{14}\text{B}$  is possibly attributable to mixing between the boron elements and the neighboring iron elements. The importance of this chemical effect has been confirmed by first-principles calculation of light elements in iron lattices<sup>10</sup>. In a recent first-principles study<sup>11</sup> on the interstitial X in  $\text{NdTiFe}_{11}\text{X}$  ( $\text{X} = \text{B}, \text{C}, \text{N}, \text{O}, \text{F}$ ), enhancement of magnetization by the magnetovolume effect and chemical effect was investigated.

Finite-temperature magnetism in hard-magnet compounds has also been studied. It was demonstrated in a study<sup>12</sup> of an ab initio spin model of  $\text{NdFe}_{12}\text{N}$  that intersite magnetic coupling between rare-earth sites (R) and transition metal sites (T) is a key factor, and magnetic anisotropy above room temperature is expected to be enhanced significantly by strengthening the R–T couplings.

In this paper, we investigate magnetic couplings in  $\text{NdFe}_{12}$  and  $\text{NdFe}_{12}\text{X}$  for  $\text{X} = \text{B}, \text{C}, \text{N}, \text{O}, \text{F}$  based on first-principles calculation. The theoretical framework and the computational methods are described in Section II. We analyze the effects of the interstitial dopant X on the magnetic couplings by using Liechtenstein’s formula. The obtained intersite magnetic couplings are converted to a Curie temperature by using the mean field approximation. The dependence of the R–T magnetic couplings on X is discussed in Section III A, and the values

of the Curie temperature are discussed in Section III B.

## II. THEORETICAL FRAMEWORK AND METHODS

We use AkaiKKR<sup>13</sup>—a program based on the Korringa–Kohn–Rostoker (KKR)<sup>14,15</sup> Green’s function method, which is also known as MACHIKANNEYAMA—for calculation of magnetic moments and intersite magnetic couplings. This calculation is performed based on the local density approximation<sup>16,17</sup>.

Spin–orbit coupling is considered at only the Nd site, with the f-electrons treated as an open core of trivalent Nd with the configuration limited by Hund’s rule (the open-core approximation<sup>18–20</sup>). We apply the self-interaction correction scheme proposed by Perdew and Zunger<sup>21</sup> to Nd-f orbitals under the self-consistent scheme. The contribution of the Nd-f electrons to values of the magnetic moment is not included in our results. The 1s–5s, 2p–4p, 3d–4d orbitals at Nd; the 1s–2s, 2p–3p orbitals at Fe; and the 1s orbital at X and the 2s orbitals at X = F are treated as core states. We consider up to d-scattering ( $l_{\max} = 2$ ) in the systems, and sample  $6 \times 6 \times 6$  k-points in the full first Brillouin zone with reduction of computational tasks by exploiting the crystal symmetry. A common set of muffin-tin radii is used in all calculations for NdFe<sub>12</sub> and NdFe<sub>12</sub>X (X = B, C, N, O, F) such that the domain volume of local potentials perturbed in Liechtenstein’s method does not depend on the system. We place one X atom per formula unit at the 2b site.

We use lattice parameters obtained via QMAS<sup>22</sup>, which is a package for first-principles calculation based on the projector augmented-wave (PAW) method<sup>23,24</sup>, within a generalized gradient approximation. These values of the lattice parameters are summarized in Appendix A. We refer readers to Ref. 25 for details of the calculation setup.

To investigate the dependence of magnetic properties on lattice parameters, we also perform calculations of hypothetical NdFe<sub>12</sub>X systems with the lattice parameters fixed to the values of other systems. We write “A#B” to mean “the system having chemical formula A with the lattice parameters of system B.” For example, we examine NdFe<sub>12</sub>#NdFe<sub>12</sub>X to investigate the effect of structural changes (lattice expansion, etc.) induced by the introduction of X separately from the chemical effects. For further simplicity, we use the ordinary chemical formulae NdFe<sub>12</sub> and NdFe<sub>12</sub>X to denote systems with the optimal structure unless otherwise stated.

Our definition of intersite magnetic couplings is as follows. According to Liechtenstein et al.<sup>26</sup>, we map energy shifts caused by spin-rotational perturbations onto  $J_{i,j}$  values in the following classical Heisenberg Hamiltonian  $\mathcal{H}$ :

$$\mathcal{H} = - \sum_i \sum_j J_{i,j} \vec{e}_i \cdot \vec{e}_j, \quad (1)$$

where  $\vec{e}_i$  is a unit vector taking the direction of the local spin moment at the  $i$ th site. It is also possible to determine a set of  $J_{i,j}$  values by comparing the total energies calculated for several different magnetic structures (e.g., different anti-ferromagnetic configurations). However, to obtain a required number of unique  $J_{i,j}$  values for a fixed magnetic structure, we exploit Liechtenstein's prescription. Our Hamiltonian can be transformed formally into the form of  $\mathcal{H} = - \sum_{i,j} \vec{S}_i \mathcal{J}_{i,j} \vec{S}_j$ , with  $J_{i,j} = S_i^0 \mathcal{J}_{i,j} S_j^0$  and  $\vec{S}_i = S_i^0 \vec{e}_i$ , where  $S_i^0$  denotes the local moment of the  $i$ th site in the ground state. Note, however, that  $\mathcal{J}_{i,j}$  is an indirect outcome from Liechtenstein's scheme, whereas  $J_{i,j}$  is more directly related to the energy shift under the perturbation at the  $i$ th and  $j$ th sites considered in the scheme. Therefore, we discuss values of  $J_{i,j}$  instead of  $\mathcal{J}_{i,j}$  to maintain theoretical clarity.

### III. RESULTS AND DISCUSSION

#### A. Chemical effects of X on $J_{R-T}$

Figure 1 shows the magnetic coupling constants  $J_{R-T}$  ( $J_{i,j}$  of R-T bonds) for NdFe<sub>12</sub> (denoted by X = Vc) and NdFe<sub>12</sub>X for X = B, C, N, O, F. There are three iron sublattices (8j, 8i, and 8f) in the ThMn<sub>12</sub> structure, and values of  $J_{R-T}$  for the shortest Nd-Fe(8j), Nd-Fe(8i), and Nd-Fe(8f) bonds are shown. The three coupling constants have similar values in NdFe<sub>12</sub>. The introduction of X changes the strengths of the couplings significantly, with the magnitudes of the changes differing considerably between the different couplings. The  $J_{\text{Nd-Fe}(8j)}$  coupling exhibits the strongest dependency on X, which is understandable because Fe(8j) is the closest site to X. The  $J_{\text{Nd-Fe}(8j)}$  coupling is reduced in all cases where X is introduced, with the exception of X = B. The smallest value is found at X = N. That value is less than half of NdFe<sub>12</sub>. In contrast,  $J_{\text{Nd-Fe}(8i)}$  and  $J_{\text{Nd-Fe}(8f)}$  are enhanced, although slightly, by N. Nitrogenation thus appears to effectively reduce the Nd-Fe coupling strengths. This suggests that nitrogenation exacerbates unfavorable thermal dumping of magnetocrystalline anisotropy, although it induces strong uniaxial anisotropy at low temperatures<sup>12</sup>.

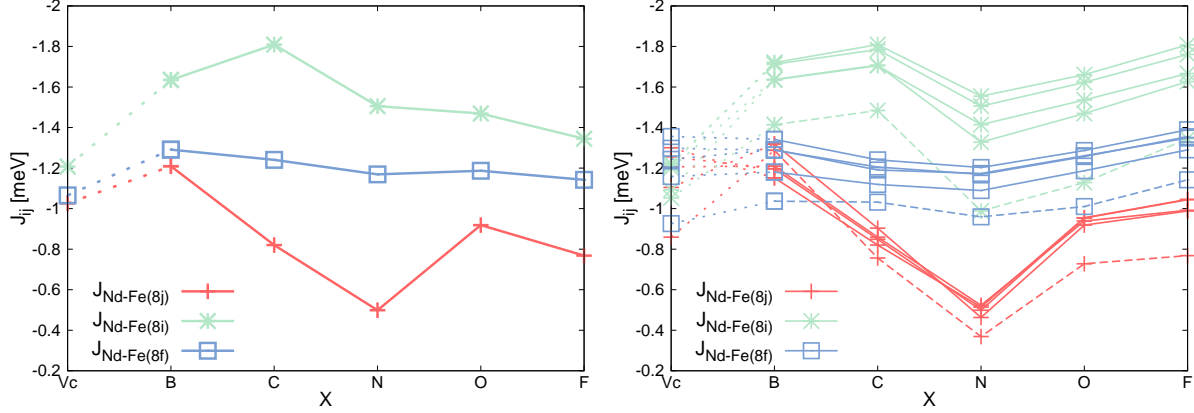


FIG. 1. (Color online) (Left) Values of  $J_{R-T}$  for  $\text{NdFe}_{12}\text{X}$  ( $X = \text{Vc}, \text{B}, \text{C}, \text{N}, \text{O}, \text{F}$ ), where  $\text{NdFe}_{12}\text{Vc}$  denotes  $\text{NdFe}_{12}$ . (Right) Values of  $J_{R-T}$  for  $\text{NdFe}_{12}\text{X}\#\text{NdFe}_{12}\text{Z}$  ( $Z = \text{B}, \text{C}, \text{N}, \text{O}, \text{F}$ ). Values of  $J_{R-T}$  calculated for the same element  $Z$  are connected by lines, with dashed lines indicating  $Z = \text{F}$ .

To examine the chemical effects separately from the structural effects, the results for  $\text{NdFe}_{12}\text{X}\#\text{NdFe}_{12}\text{Z}$  ( $Z = \text{B}, \text{C}, \text{N}, \text{O}, \text{F}$ ) are plotted in the right panel of Fig. 1. It can be seen that the overall trends as a function of  $X$  are not highly dependent on  $Z$ . This indicates that chemical effects dominate this behavior. Looking at the results in more detail, it can be seen that each of the absolute values of the  $J_{R-T}$  constants has its minimum at  $X = \text{N}$  notwithstanding the choice of lattice parameters. Furthermore, the reductions caused by  $\text{N}$  are smaller than the fluctuations due to the structural changes in the cases of  $J_{\text{Nd}-\text{Fe}(8i)}$  and  $J_{\text{Nd}-\text{Fe}(8f)}$ . However, the reduction in  $J_{\text{Nd}-\text{Fe}(8j)}$  due to  $\text{N}$  is too large to be overcome by the structural effect.

Figure 2 shows  $J_{\text{Nd}-\text{Fe}(8j)}$  for  $\text{NdFe}_{12}\text{X}\#\text{NdFe}_{12}\text{N}$  with fractional changes to the atomic number of  $X$ ,  $Z_X$ . This perturbation on  $Z_X$  serves as a theoretical probe to the system, and the external potential with the fractional  $Z_X$  can also be interpreted as a model within the virtual crystal approximation for random occupation of the  $X$  site by multiple elements with the mean value of their atomic numbers coinciding with  $Z_X$ . In Fig. 2, there is a significant decrease of the magnitude at approximately  $Z_X = 7$  ( $X = \text{N}$ ), with a minimum at  $Z_X = 6.8$ . The figure also shows the local spin moment at the  $\text{Nd}$  site as a function of  $Z_X$ . This local moment is strongly correlated with  $J_{\text{Nd}-\text{Fe}(8j)}$ , so the reduction in  $J_{\text{Nd}-\text{Fe}(8j)}$  by nitrogenation is attributable to the reduction in the spin magnetic moment at the  $\text{Nd}$  site. Note that  $J_{\text{Nd}-\text{Fe}(8j)}$  does not necessarily change proportionally to the local moments because  $\mathcal{J}_{i,j}$  in

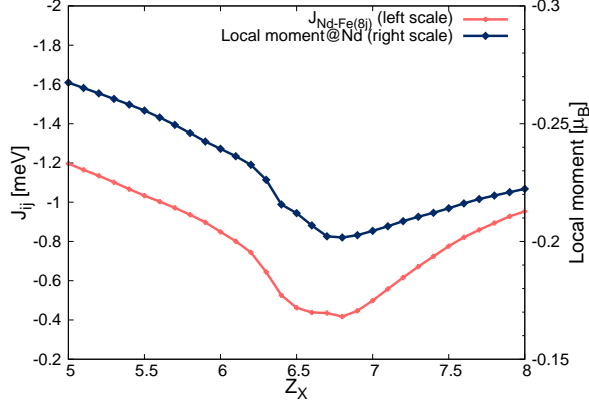


FIG. 2. (Color online)  $J_{\text{Nd-Fe}(8j)}$  (left scale) for  $\text{NdFe}_{12}\text{X}\#\text{NdFe}_{12}\text{N}$  as a function of  $Z_X$  — the atomic number of X — compared with the local moment of the Nd site (right scale). Note that the right scale for the local moments is inverted.

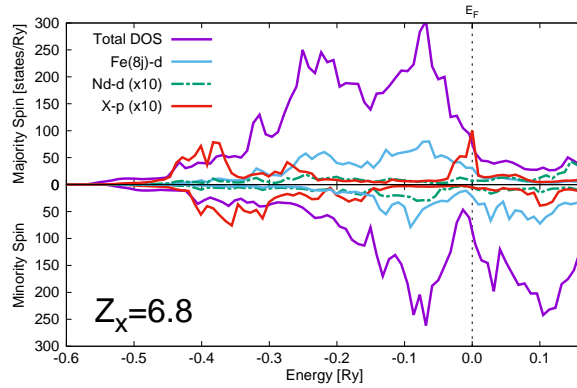


FIG. 3. (Color online) Total and partial DOS of  $\text{NdFe}_{12}\text{X}\#\text{NdFe}_{12}\text{N}$  at  $Z_X = 6.8$ . Note that the partial densities of the Nd-d states and the X-p states are magnified tenfold.

$J_{i,j} = S_i^0 \mathcal{J}_{i,j} S_j^0$  also depends on the ground state of the system.

Figure 3 plots the density of states (DOS) at  $Z_X = 6.8$ . The X-p DOS has a peak at the Fermi level in the majority-spin channel, but there is no feature in the minority channel at that point. This type of DOS distribution has been discussed previously<sup>10,11,27</sup> to explain the change in the total spin moment caused by X. The discussion is also useful for understanding the reduction of the Nd moment, and the results of our calculation also show good agreement with the accompanying theory. The X-2p state hybridizes with states of the neighboring Fe sites. An antibonding state between them appears above the Fermi level in the cases of X = B and X = C. As  $Z_X$  increases, the X-2p level becomes deeper. Consequently, this hybridized state is pulled down (Fig. 4) and crosses the Fermi level at  $Z_X \sim 7$  in the

majority-spin channel, which leads to enhancement of the magnetic moment of the whole compound (although the magnetovolume effect also enhances the magnetic moment, the dependence of the total moment on X comes mainly from the chemical effect<sup>11</sup>).

This hybridized state in the majority-spin channel has some weight at the Nd site. Hence, as the occupation number of this state increases, the majority-spin density becomes larger. This results in a decrease in the magnitude of the local spin moment at the Nd site because it is antiparallel to the total spin moment (electrons in the majority-spin channel of the entire system are a minority at the Nd site). This reduction leads to weakening of the spin-rotational perturbation considered in Liechtenstein’s formula and weakens  $J_{\text{Nd-Fe}(8j)}$ . To summarize, filling of the hybridized state affects both the magnetization and the Nd–Fe magnetic coupling, but in opposite ways.

## B. Chemical effect of X on the Curie temperature

All values of the Curie temperature are computed within the mean-field approximation from  $J_{i,j}$ . We use two different sets of  $J_{i,j}$  for comparison. The larger set,  $\mathcal{L}$ , is composed of  $J_{i,j}$  for the bonds with lengths shorter than  $0.9a$ , where  $a$  is the side length of the base square for the conventional unit cell. The smaller set,  $\mathcal{S}$ , is the union of the following two subsets: (i)  $J_{i,j}$  for the shortest bonds in the classes of the site combinations (e.g., Fe(8j)–Fe(8i), Fe(8f)–Nd and X–X); and (ii)  $J_{i,j}$  for the bonds shorter than 3.80 Å. The geometries of the T–T and R–T bonds in  $\mathcal{S}$  are shown in Fig. 5. As a result, all bonds between the Fe’s and their 3rd nearest Fe-neighbors are included in  $\mathcal{S}$ . When deciding on this cutoff of 3.80 Å, we referred to a previous Monte Carlo study of Nd<sub>2</sub>Fe<sub>14</sub>B (Ref. 28), where results with a cutoff of 3.52 Å are in good agreement with results calculated with a cutoff of 15.8 Å.

Figure 6 shows the Curie temperatures of NdFe<sub>12</sub> and NdFe<sub>12</sub>X obtained from the sets  $\mathcal{L}$  (left) and  $\mathcal{S}$  (right). Results for NdFe<sub>12</sub>#NdFe<sub>12</sub>X are also presented. The overall behavior of the two curves is similar between the two panels, which would justify our use of the smaller set  $\mathcal{S}$  in the analysis of  $J_{i,j}$  dependence of the Curie temperatures appearing later. The Curie temperature is enhanced by the introduction of X in all cases studied. Comparing the results for NdFe<sub>12</sub>X with NdFe<sub>12</sub>#NdFe<sub>12</sub>X, it can be seen that the enhancement originates primarily from the structure as for X = C. The same order of enhancement originating from the structural change (mainly the volume expansion) is also seen in the cases of X = B, N, O,

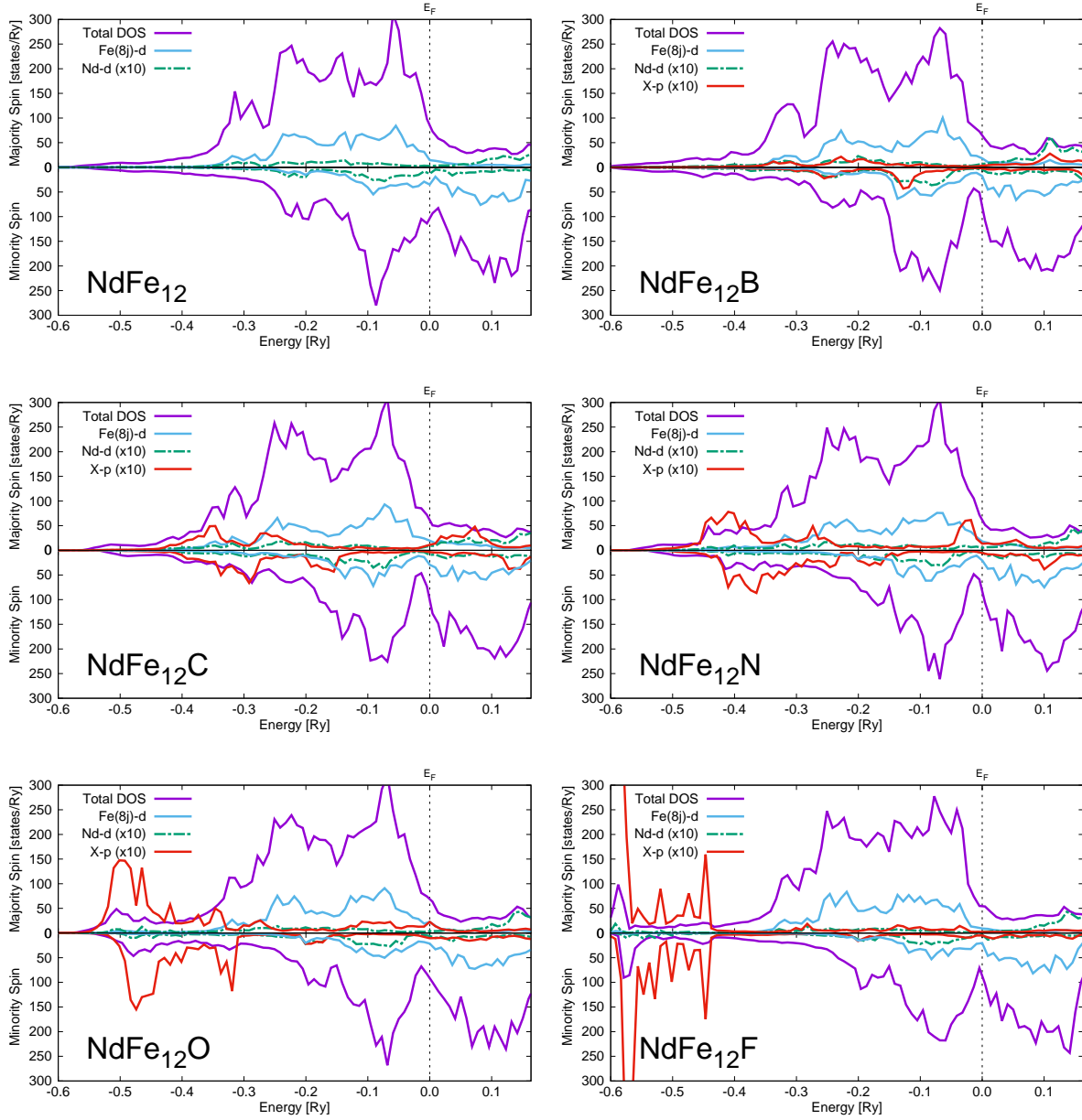


FIG. 4. (Color online) Total and partial DOS of  $\text{NdFe}_{12}$  and  $\text{NdFe}_{12}\text{X}$  ( $\text{X} = \text{B}, \text{C}, \text{N}, \text{O}, \text{F}$ ). Note that the partial density values of the Nd-d states and the X-p states are multiplied by 10 to show the detail of the curves.

F. However, the structural change accounts only for approximately half of the enhancement. The chemical effects are as important as the structural change.

The Curie temperature of  $\text{NdFe}_{12}\text{N}$  shown in Fig. 6 is much higher than the experimental value of  $T_C \approx 820$  K obtained by Hirayama et al.<sup>1</sup>. This overestimation in our calculation presumably comes from the use of the mean field approximation, which almost certainly



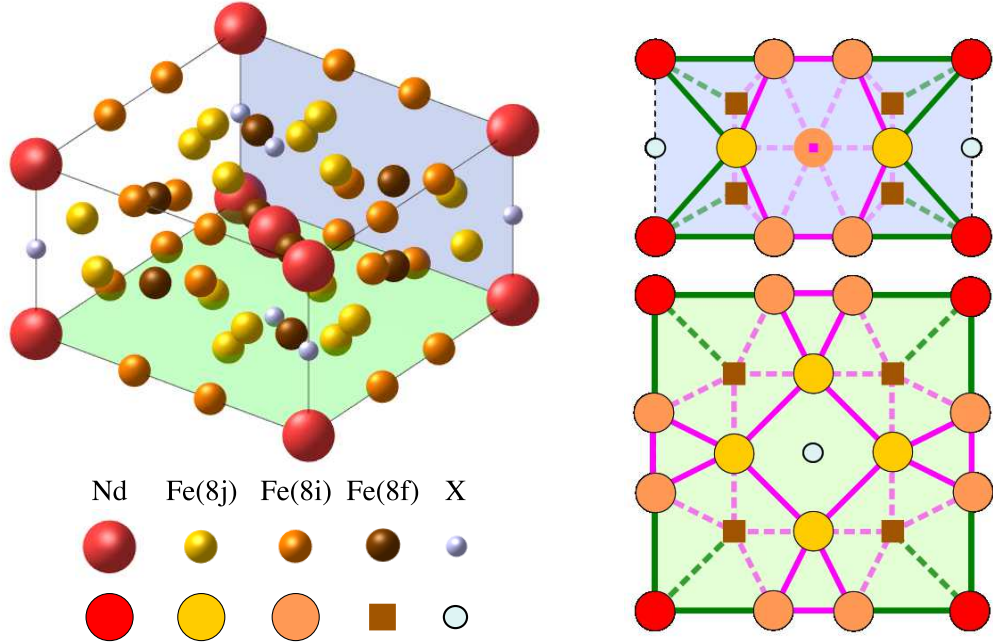


FIG. 5. (Color online) Crystal structure of  $\text{NdFe}_{12}\text{X}$ . The left figure shows the conventional unit cell of the structure. The right figures show cross sections of the cell with the  $ab$ - and  $ac$ -planes indicated by light blue and green, respectively, in the left figure. The T–T bonds (magenta) and the R–T bonds (green) in the smaller set,  $\mathcal{S}$ , are also shown. Solid lines indicate in-plane bonds, and dashed lines indicate out-of-plane bonds.

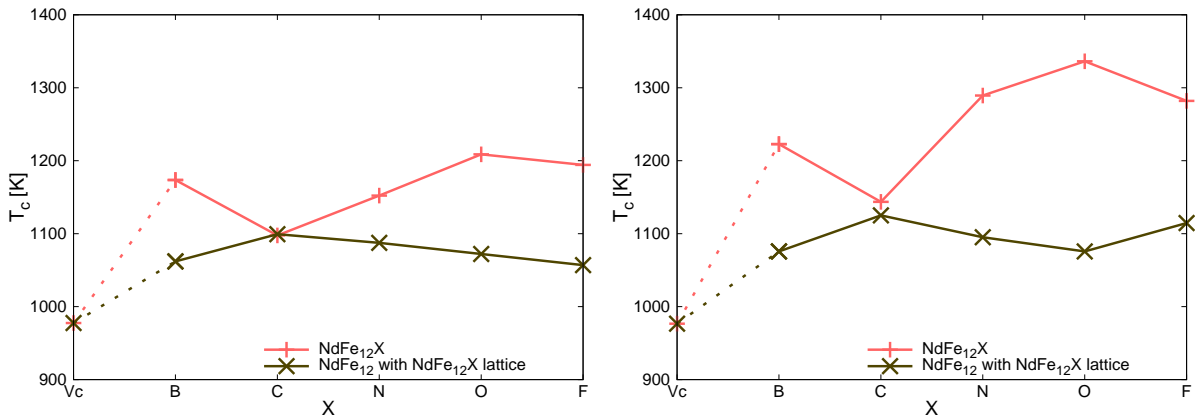


FIG. 6. (Color online) The Curie temperature of  $\text{NdFe}_{12}\text{X}$  ( $X = \text{Vc}, \text{B}, \text{C}, \text{N}, \text{O}, \text{F}$ ) with the optimized lattices (+ symbols) and  $\text{NdFe}_{12}\#\text{NdFe}_{12}\text{X}$  (x symbols).  $\text{NdFe}_{12}\text{Vc}$  denotes  $\text{NdFe}_{12}$ . The data in the left figure are calculated from the larger  $J_{i,j}$  set,  $\mathcal{L}$ ; the data in the right figure are calculated from the smaller set,  $\mathcal{S}$ .

overestimates  $T_C$  of spin models. However, the calculated difference between  $T_C$  before and after the nitrogenation is comparable to the experimental value of  $T_C^{\text{NdTiFe}_{11}\text{N}_x} - T_C^{\text{NdTiFe}_{11}} \approx 200$  K based on  $T_C^{\text{NdTiFe}_{11}\text{N}_x}$  from Ref. 6 and  $T_C^{\text{NdTiFe}_{11}}$  from Ref. 29.

To see how the Curie temperature depends on the change in  $J_{i,j}$  caused by the introduction of X, we calculate the following quantity:

$$\Delta T_C^{(k,l)} = T_C[\{J_{i,j}^{\text{NdFe}_{12}\text{X}}\}] - T_C[\{J_{i,j}^{\text{LOU},(k,l)}\}], \quad (2)$$

where  $T_C[\{J_{i,j}\}]$  is the Curie temperature calculated from the set of magnetic couplings  $\{J_{i,j}\}$ , and  $J_{i,j}^{\text{LOU},(k,l)}$  is defined as follows:

$$J_{i,j}^{\text{LOU},(k,l)} = \begin{cases} J_{i,j}^{\text{NdFe}_{12}} & [(i,j) \text{ is equivalent to } (k,l)] \\ J_{i,j}^{\text{NdFe}_{12}\text{X}} & (\text{otherwise}) \end{cases}, \quad (3)$$

where LOU stands for “leave-one-unchanged.” Note that this  $\Delta T_C^{(k,l)}$  is positive when the change in  $J_{k,l}$  caused by the introduction of X enhances the Curie temperature. We also use a similar quantity  $\tilde{\Delta T}_C^{(k,l)}$  by replacing  $J_{i,j}$  in the reference NdFe<sub>12</sub> system in equation (3) with the values from NdFe<sub>12</sub>#NdFe<sub>12</sub>X. In this analysis, we focus on the bonds in  $\mathcal{S}$  and use only their  $J_{i,j}$  values to calculate  $\Delta T_C^{(k,l)}$ .

The left panel in Fig. 7 shows  $\Delta T_C^{(k,l)}$  as a function of X. There are two Fe(8i)–Fe(8i) bonds and two Fe(8j)–Fe(8i) bonds in the  $\mathcal{S}$  subset. To distinguish one from the other, we denote the shortest bonds by <i> and the second-shortest bonds by <ii> in Fig. 7 and the following discussion. From Fig. 7, it can be seen that the values of  $\Delta T_C^{\text{T-T}}$  ( $\Delta T_C^{(k,l)}$  for T–T bonds) are much larger than the values of  $\Delta T_C^{\text{R-T}}$  and  $\Delta T_C^{\text{R-R}}$ , which are denoted by “Others” in the figure. This indicates that changes in the T–T bonds predominantly cause the enhancement of  $T_C$ . The right panel in Fig. 7 shows  $\tilde{\Delta T}_C^{(k,l)}$ . We do not find any significant differences between  $\Delta T_C^{(k,l)}$  and  $\tilde{\Delta T}_C^{(k,l)}$ , which indicates that the chemical effects significantly contribute to  $\Delta T_C^{(k,l)}$ , whereas the structure change plays a minor role.

Both  $\Delta T_C^{\text{Fe}(8j)\text{--Fe}(8f)}$  and  $\tilde{\Delta T}_C^{\text{Fe}(8j)\text{--Fe}(8f)}$  have the largest magnitude in the range of X = B–O. This implies that the change of  $J_{\text{Fe}(8j)\text{--Fe}(8f)}$  caused by the introduction of X has a strong positive effect on the enhancement of the Curie temperature. It is noteworthy that even at X = C, where the lattice expansion alone seems sufficient to explain the enhancement of the Curie temperature,  $\tilde{\Delta T}_C^{\text{Fe}(8j)\text{--Fe}(8f)}$  is large and not very different from that at X = B, N, O. Therefore, whereas the change in  $J_{\text{Fe}(8j)\text{--Fe}(8f)}$  gives the largest contribution, it does not

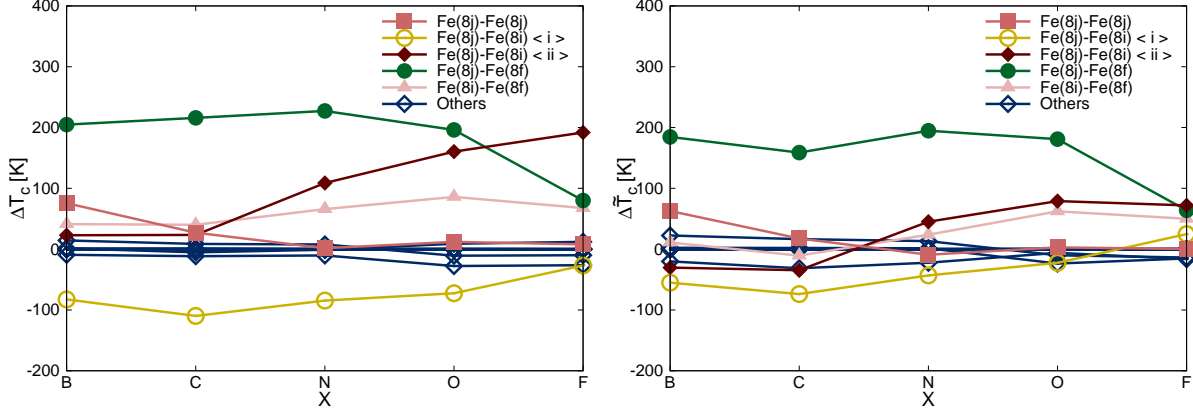


FIG. 7. (Color online) (Left) Difference in Curie temperature  $\Delta T_C^{(k,l)}$  as defined by equation (2), and (Right)  $\tilde{\Delta T}_C^{(k,l)}$  in which the lattice parameters of the reference  $\text{NdFe}_{12}$  system [see the first line in Eq. (3)] are set to the parameters of  $\text{NdFe}_{12}\text{X}$ .

explain the dependence of the Curie temperature on X. In the case of  $X = \text{B}$ , the difference from  $X = \text{C}$  mainly comes from the increase in  $\tilde{\Delta T}_C^{\text{Fe}(8j)-\text{Fe}(8j)}$ , whereas in the case of  $X = \text{N}$ , O, F, it comes mainly from the increase in  $\tilde{\Delta T}_C^{\text{Fe}(8j)-\text{Fe}(8i)<ii>}$  and  $\tilde{\Delta T}_C^{\text{Fe}(8i)-\text{Fe}(8f)}$ . This leads us to believe that the mechanism behind the enhancement of the Curie temperature differs between the case of  $X = \text{B}$  and those of  $X = \text{N}$ , O, F.

#### IV. CONCLUSION

We studied and investigated the internal magnetic couplings of  $\text{NdFe}_{12}$  and  $\text{NdFe}_{12}\text{X}$  for  $X = \text{B}, \text{C}, \text{N}, \text{O}, \text{F}$  by first-principles calculations and found that the introduction of nitrogen to  $\text{NdFe}_{12}$  reduces the strength of R-T magnetic couplings owing to Nd-X hybridization, with  $J_{\text{Nd}-\text{Fe}(8j)}$  particularly reduced so significantly that lattice expansion due to the nitrogen cannot compensate for the reduction. Although nitrogen is often used to enhance the magnetic properties of magnetic compounds, our results suggest that nitrogenation may have countereffects on the anisotropy field of  $\text{NdFe}_{12}$  at finite temperatures.

We also evaluated the Curie temperatures of  $\text{NdFe}_{12}$  and  $\text{NdFe}_{12}\text{X}$  within the mean field approximation and found that the volume expansion caused by the introduction of X cannot explain all enhancement of  $T_C$ . The introduction of X causes significant changes in the magnetic couplings of  $\text{NdFe}_{12}$  and has a significant effect on the Curie temperature. Nitrogen was found to enhance the Curie temperature, as found experimentally in similar

compounds. Oxygen and fluorine were also found to enhance  $T_C$  as much as nitrogen. Although boron also produced the same order of positive effect on  $T_C$  within the framework above (see also Appendix B2 for results with a model for the paramagnetic state), the mechanism appears to be different from that for the cases of  $X = \text{N, O, F}$ .

## ACKNOWLEDGMENTS

The authors are grateful for support from the Elements Strategy Initiative Project under the auspices of MEXT. This work was also supported by MEXT as a social and scientific priority issue (Creation of new functional Devices and high-performance Materials to Support next-generation Industries; CDMSI) to be tackled by using the post-K computer. The computation was partly carried out using the facilities of the Supercomputer Center, the Institute for Solid State Physics, the University of Tokyo, and the supercomputer of AC-CMS, Kyoto University. This research also used computational resources of the K computer provided by the RIKEN Advanced Institute for Computational Science through the HPCI System Research project (Project ID:hp170100).

## Appendix A: Lattice parameters

Table I shows the optimized lattice parameters for  $\text{NdFe}_{12}$  and  $\text{NdFe}_{12}\text{X}$  ( $X = \text{B, C, N, O, F}$ ) that we used in our calculations. The parameters  $p_{8i}$  and  $p_{8j}$  correspond to the atomic positions described in table II.

TABLE I. Optimized lattice parameters for  $\text{NdFe}_{12}\text{X}$  ( $X = \text{Vc, B, C, N, O, F}$ ), where  $\text{NdFe}_{12}\text{Vc}$  denotes  $\text{NdFe}_{12}$ . For the definitions of the inner parameters  $p_{8j}$  and  $p_{8i}$ , see table II.

$X$	$a$ [ $\text{\AA}$ ]	$c$ [ $\text{\AA}$ ]	$p_{8i}$	$p_{8j}$
Vc	8.533	4.681	0.3594	0.2676
B	8.490	4.933	0.3599	0.2683
C	8.480	4.925	0.3606	0.2756
N	8.521	4.883	0.3612	0.2742
O	8.622	4.794	0.3608	0.2670
F	8.782	4.720	0.3594	0.2487

TABLE II. Atomic positions of the elements assumed in our calculation for  $\text{NdFe}_{12}$  and  $\text{NdFe}_{12}\text{X}$  ( $\text{X} = \text{B}, \text{C}, \text{N}, \text{O}, \text{F}$ ). The variables,  $x$ ,  $y$ , and  $z$  denote the point  $(ax, ay, cz)$  in Cartesian coordinates.

Element	Site	$x$	$y$	$z$
Nd	2a	0	0	0
Fe	8f	0.25	0.25	0.25
Fe	8i	$p_{8i}$	0	0
Fe	8j	$p_{8j}$	0.5	0
X	2b	0	0	0.5

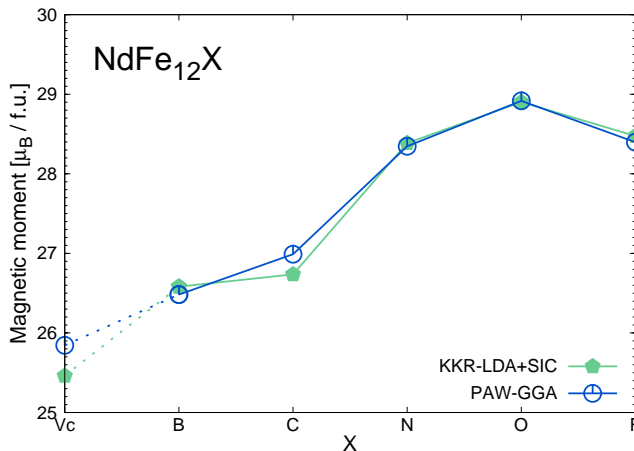


FIG. 8. (Color online) Total magnetic moment of  $\text{NdFe}_{12}\text{X}$  ( $\text{X} = \text{Vc}, \text{B}, \text{C}, \text{N}, \text{O}, \text{F}$ ), where  $\text{NdFe}_{12}\text{Vc}$  denotes  $\text{NdFe}_{12}$ .

## Appendix B: Total and local moments

### 1. Comparison with full-potential calculation

Figure 8 shows the total moment of  $\text{NdFe}_{12}$  and  $\text{NdFe}_{12}\text{X}$  ( $\text{X} = \text{B}, \text{C}, \text{N}, \text{O}, \text{F}$ ); Fig. 9 shows the local moments of  $\text{NdFe}_{12}$  and  $\text{NdFe}_{12}\text{X}$  ( $\text{X} = \text{B}, \text{C}, \text{N}, \text{O}, \text{F}$ ). In both, the values from KKR-LDA+SIC are compared with those from the full-potential calculation with PAW-GGA. In both cases, the regions of integration to obtain the local moments are set to the spheres with the muffin-tin radii used in the KKR calculation. The contribution from Nd-f orbitals are excluded in those plots as mentioned in section II of the main text.

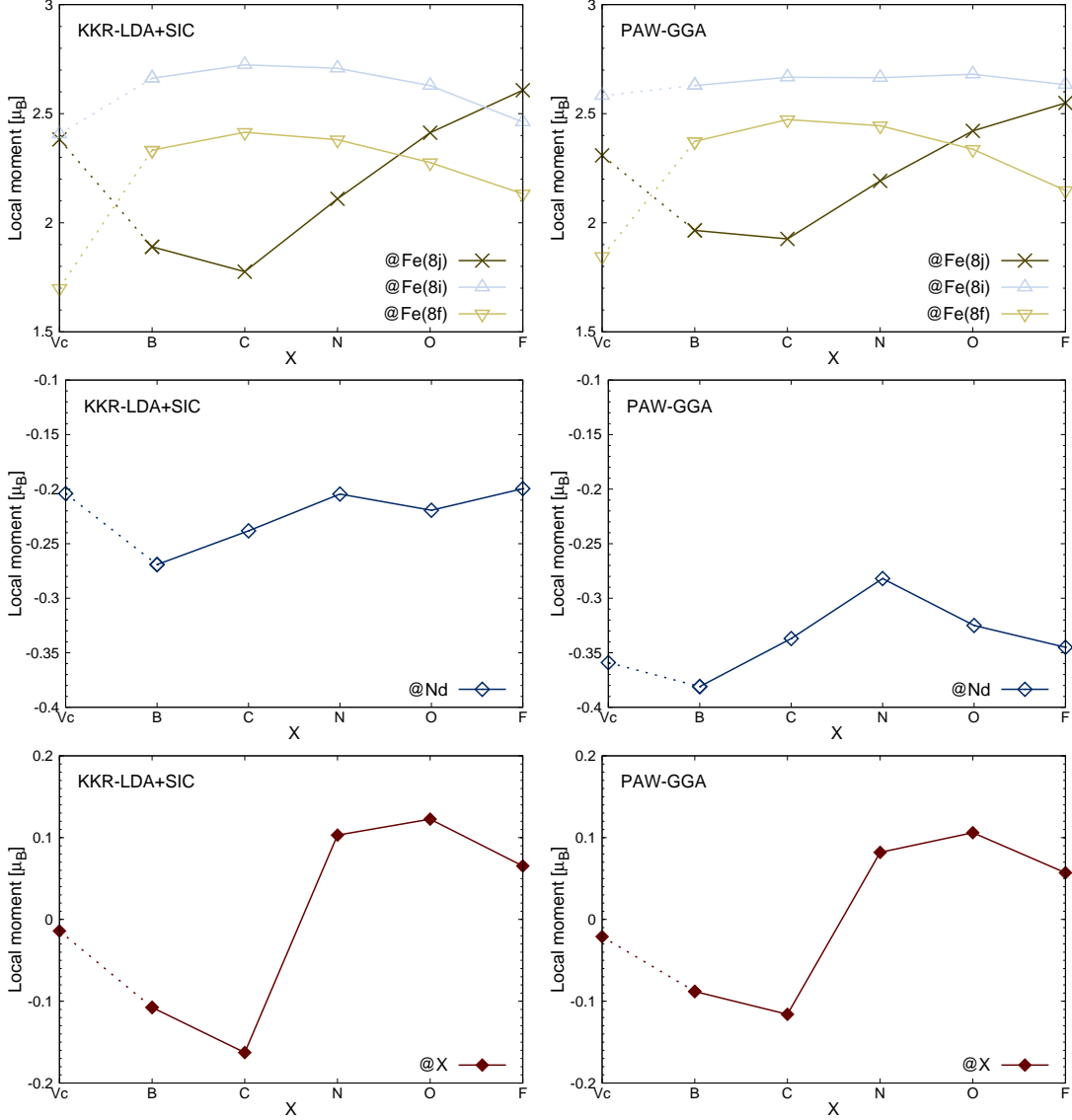


FIG. 9. (Color online) Local magnetic moments at the Fe sites (top), the Nd site (middle), and the X site (bottom) in NdFe<sub>12</sub>X (X = Vc, B, C, N, O, F), where NdFe<sub>12</sub>Vc denotes NdFe<sub>12</sub>. The data in the left figures are from the KKR-LDA+SIC calculation; the data in the right figures are from the PAW-GGA calculation with the local moments defined as integrated spin density within the muffin-tin radii used in the KKR calculation.

## 2. Local moment disorder

We also performed calculations for NdFe<sub>12</sub> and NdFe<sub>12</sub>X with the local moment disorder (LMD) model<sup>30</sup> to approximate the paramagnetic states. In the calculation, each of the atomic sites,  $\mathcal{A}$  (=Nd, Fe, X), is described by twofold atomic potentials,  $\mathcal{A}^\uparrow$  and  $\mathcal{A}^\downarrow$ , where  $\mathcal{A}^\uparrow$  has opposite spin-polarization to  $\mathcal{A}^\downarrow$ , and they are treated as potentials of distinct atoms

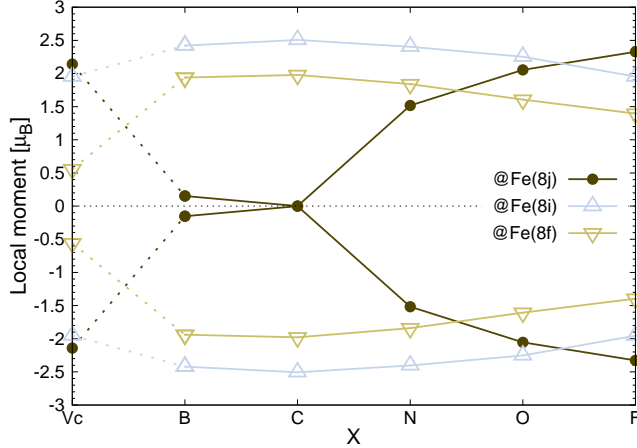


FIG. 10. (Color online) Values of the local magnetic moments at the Fe sites for  $\text{NdFe}_{12}$  (at  $X = \text{Vc}$ ) and  $\text{NdFe}_{12}\text{X}$  ( $X = \text{B}, \text{C}, \text{N}, \text{O}, \text{F}$ ) in the state of local moment disorder<sup>30</sup>.

that can occupy the  $\mathcal{A}$  site with 50% probability. This randomness is treated with the coherent potential approximation. In this hypothetical  $(\text{Nd}_{0.5}^{\uparrow}\text{Nd}_{0.5}^{\downarrow})(\text{Fe}_{0.5}^{\uparrow}\text{Fe}_{0.5}^{\downarrow})_{12}\text{X}_{0.5}^{\uparrow}\text{X}_{0.5}^{\downarrow}$  system, the absolute value of the Fe(8j) moment is greatly reduced for  $X = \text{B}$  and  $\text{C}$  as shown in Fig. 10. In contrast, for  $X = \text{N}, \text{O}, \text{F}$ , the reduction is much smaller.

Intersite magnetic couplings in this system can be compared with  $J_{i,j}$  in the main text by using Liechtenstein’s  $J_{i,j}$  between  $\mathcal{A}_i^{\uparrow}$  and  $\mathcal{A}_j^{\uparrow}$  embedded in this model system. To compare them in terms of temperature, we show the Curie temperature for  $\text{NdFe}_{12}$  and  $\text{NdFe}_{12}\text{X}$  calculated from the thus defined  $J_{i,j}$  in Fig. 11. The cutoff bond length for this  $J_{i,j}$  is  $0.9a$ , which is identical to that for  $\mathcal{L}$  in Section III B. Whereas the fluctuation at the Fe(8j) site seems to offset the enhancement of magnetism in the case of  $X = \text{B}, \text{C}$ , the exchange interaction in  $X = \text{N–F}$  and  $\text{Vc}$  ( $\text{NdFe}_{12}$ ) seems robust.

## REFERENCES

- <sup>1</sup>Y. Hirayama, Y. Takahashi, S. Hirosawa, and K. Hono, “ $\text{NdFe}_{12}\text{N}_x$  hard-magnetic compound with high magnetization and anisotropy field,” *Scripta Materialia* **95**, 70–72 (2015).
- <sup>2</sup>Y. Hirayama, T. Miyake, and K. Hono, “Rare-earth lean hard magnet compound  $\text{NdFe}_{12}\text{N}$ ,” *JOM* **67**, 1344–1349 (2015).
- <sup>3</sup>T. Miyake, K. Terakura, Y. Harashima, H. Kino, and S. Ishibashi, “First-principles study of magnetocrystalline anisotropy and magnetization in  $\text{NdFe}_{12}$ ,  $\text{NdFe}_{11}\text{Ti}$ , and  $\text{NdFe}_{11}\text{TiN}$ ,” *Journal of the Physical Society of Japan* **83**, 043702 (2014).

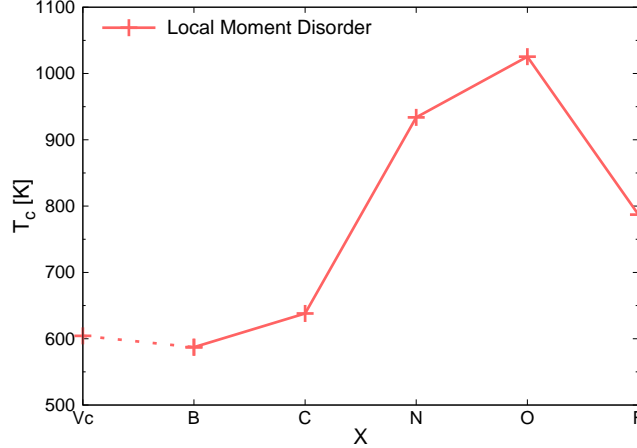


FIG. 11. (Color online) Values of the Curie temperature for  $\text{NdFe}_{12}$  (at  $X = \text{Vc}$ ) and  $\text{NdFe}_{12}\text{X}$  ( $X = \text{B, C, N, O, F}$ ) in the state of local moment disorder<sup>30</sup>.

<sup>4</sup>H. Sun, B.-P. Hu, H.-S. Li, and J. Coey, “Magnetic properties of  $\text{Y}_2\text{Fe}_{17}\text{C}_x$ ,” *Solid State Communications* **74**, 727–730 (1990).

<sup>5</sup>J. Coey and H. Sun, “Improved magnetic properties by treatment of iron-based rare earth intermetallic compounds in ammonia,” *Journal of Magnetism and Magnetic Materials* **87**, L251–L254 (1990).

<sup>6</sup>Y.-c. Yang, X.-d. Zhang, L.-s. Kong, Q. Pan, and S.-l. Ge, “New potential hard magnetic material— $\text{NdTiFe}_{11}\text{N}_x$ ,” *Solid state communications* **78**, 317–320 (1991).

<sup>7</sup>Y.-c. Yang, X.-d. Zhang, S.-l. Ge, Q. Pan, L.-s. Kong, H. Li, J.-l. Yang, B.-s. Zhang, Y.-f. Ding, and C.-t. Ye, “Magnetic and crystallographic properties of novel fe-rich rare-earth nitrides of the type  $\text{RTiFe}_{11}\text{N}_{1-\delta}$ ,” *Journal of applied physics* **70**, 6001–6005 (1991).

<sup>8</sup>J. Kanamori, “Interplay between electronic structure and correlation through the sd mixing in transition metal systems,” *Progress of Theoretical Physics Supplement* **101**, 1–10 (1990).

<sup>9</sup>J. Kanamori, “Rare earth elements and magnetism in metallic systems,” *Journal of alloys and compounds* **408**, 2–8 (2006).

<sup>10</sup>H. Akai, M. Takeda, M. Takahashi, and J. Kanamori, “Roles of light interstitials in magnetism of fe,” *Solid state communications* **94**, 509–513 (1995).

<sup>11</sup>Y. Harashima, K. Terakura, H. Kino, S. Ishibashi, and T. Miyake, “Nitrogen as the best interstitial dopant among  $X=\text{B, C, N, O}$ , and  $\text{F}$  for strong permanent magnet  $\text{NdFe}_{11}\text{TiX}$ : First-principles study,” *Phys. Rev. B* **92**, 184426 (2015).

<sup>12</sup>M. Matsumoto, H. Akai, Y. Harashima, S. Doi, and T. Miyake, “Rele-



- vance of 4f-3d exchange to finite-temperature magnetism of rare-earth permanent magnets: An ab-initio-based spin model approach for ndfe12n,” *Journal of Applied Physics* **119**, 213901 (2016), <http://dx.doi.org/10.1063/1.4952989>.
- <sup>13</sup>“AkaiKKR(Machikaneyama),” <http://kkk.issp.u-tokyo.ac.jp>.
- <sup>14</sup>J. Korringa, “On the calculation of the energy of a bloch wave in a metal,” *Physica* **13**, 392–400 (1947).
- <sup>15</sup>W. Kohn and N. Rostoker, “Solution of the schrödinger equation in periodic lattices with an application to metallic lithium,” *Phys. Rev.* **94**, 1111–1120 (1954).
- <sup>16</sup>P. Hohenberg and W. Kohn, “Inhomogeneous electron gas,” *Physical Review* **136**, B864 (1964).
- <sup>17</sup>W. Kohn and L. J. Sham, “Self-consistent equations including exchange and correlation effects,” *Physical Review* **140**, A1133 (1965).
- <sup>18</sup>J. Jensen and A. R. Mackintosh, *Rare earth magnetism* (Clarendon Oxford, 1991).
- <sup>19</sup>M. Richter, “Band structure theory of magnetism in 3d-4f compounds,” *Journal of Physics D: Applied Physics* **31**, 1017 (1998).
- <sup>20</sup>I. L. M. Locht, Y. O. Kvashnin, D. C. M. Rodrigues, M. Pereiro, A. Bergman, L. Bergqvist, A. I. Liechtenstein, M. I. Katsnelson, A. Delin, A. B. Klautau, B. Johansson, I. Di Marco, and O. Eriksson, “Standard model of the rare earths analyzed from the hubbard i approximation,” *Phys. Rev. B* **94**, 085137 (2016).
- <sup>21</sup>J. P. Perdew and A. Zunger, “Self-interaction correction to density-functional approximations for many-electron systems,” *Phys. Rev. B* **23**, 5048–5079 (1981).
- <sup>22</sup>“QMAS—Quantum MAterials Simulator Official Site,” <http://qmas.jp>.
- <sup>23</sup>P. E. Blöchl, “Projector augmented-wave method,” *Phys. Rev. B* **50**, 17953–17979 (1994).
- <sup>24</sup>G. Kresse and D. Joubert, “From ultrasoft pseudopotentials to the projector augmented-wave method,” *Phys. Rev. B* **59**, 1758–1775 (1999).
- <sup>25</sup>Y. Harashima, K. Terakura, H. Kino, S. Ishibashi, and T. Miyake, “First-principles study of structural and magnetic properties of R(Fe,Ti)<sub>12</sub> and R(Fe,Ti)<sub>12</sub>N (R= Nd, Sm, Y),” in *Proceedings of Computational Science Workshop 2014 (CSW2014)*, JPS Conference Proceedings, Vol. 5 (2015) p. 1021.
- <sup>26</sup>A. I. Liechtenstein, M. Katsnelson, V. Antropov, and V. Gubanov, “Local spin density functional approach to the theory of exchange interactions in ferromagnetic metals and alloys,” *Journal of Magnetism and Magnetic Materials* **67**, 65–74 (1987).

- <sup>27</sup>S. Asano, S. Ishida, and S. Fujii, “Electronic structures and improvement of magnetic properties of  $RFe_{12}X$  ( $R= Y, Ce, Gd$ ;  $X= N, C$ ),” *Physica B: Condensed Matter* **190**, 155–168 (1993).
- <sup>28</sup>Y. Toga, M. Matsumoto, S. Miyashita, H. Akai, S. Doi, T. Miyake, and A. Sakuma, “Monte carlo analysis for finite-temperature magnetism of  $Nd_2Fe_{14}B$  permanent magnet,” *Phys. Rev. B* **94**, 174433 (2016).
- <sup>29</sup>B.-P. Hu, H.-S. Li, J. Gavigan, and J. Coey, “Intrinsic magnetic properties of the iron-rich ThMn12-structure alloys  $R(Fe_{11}Ti)$ ;  $R= Y, Nd, Sm, Gd, Tb, Dy, Ho, Er, Tm$  and  $Lu$ ,” *Journal of Physics: Condensed Matter* **1**, 755 (1989).
- <sup>30</sup>H. Akai and P. Dederichs, “Local moment disorder in ferromagnetic alloys,” *Physical Review B* **47**, 8739 (1993).